A Deep Learning Framework for Autonomous Retinal Blood Vessel Segmentation on Fluorescein Angiography

[1] Vishal Balaji Sivaraman,
Electrical and Computer Engneering,
University of Florida,
Gainesville, United States,
vi.sivaraman@ufl.edu

***Abstract*— Retina is essential for perceiving and comprehending the order of things. This essential tissue is responsible for transforming the image of the external environment into neural impulses that are transmitted to the brain. Moreover, this tissue is maintained by innumerable minute blood capillaries known as arteries and veins that circulate and detoxify vital blood levels, underlining the nuances of the whole process. It is primarily via the capillaries that oxygen and nutrients leave the blood and enter the retina, while carbon dioxide and waste materials leave the retina and enter the blood to be disposed. Moreover, these capillaries join up to form branch veins and these then join at the optic nerve to form the central retinal vein that dives into the optic nerve on its way towards the heart. Notably, each portion of the retina is supplied and discharged by a single artery and vein. As a result, if a single retinal vein or artery becomes obstructed, only the portion of the retina and visual field served by that blood vessel is affected continually, emphasizing the significance of blood vessels in the whole process. In addition, it can be concluded that the majority of abnormalities caused by retinal diseases are the result of obstructed or seeping retinal blood vessels. In an effort to address this issue, machine learning and deep learning researchers in the field of medical imaging devised a novel solution dubbed Retinal Blood Vessels Segmentation, with the primary objective of segmenting vital retinal blood vessels present in the eye. The proposed project provides a comprehensive overview of segmenting vital retinal blood vessels using an innovative technique termed UNet on Fluorescein Angiography, also known as Fundus Scans, to interpret and monitor blood flow in these vital blood vessels. In addition, this research will assist in evaluating the merits and drawbacks of the proposed technique based on its efficacy on a proprietary database and its applicability to a variety of Machine Learning environments.**

Keywords—Retinal Blood Vessels; Segmentation; Fundus Scans;DataModeling;UNet;Metrics;DiceCoefficient;DiceLoss;Intersection over Union(IoU).

I. INTRODUCTION

The retina [1] is the uppermost of the eye's three layers. This layer is responsible for transforming pertinent information from the external environment's image into neural impulses that are transmitted to the brain. Inner neurosensory retina and retinal pigment epithelium (RPE) are the two primary layers that compose the retina. In addition, sensory retina develops from the interior layer of the neuroectoderm, while RPE develops from the outer layer. The RPE is continuous anteriorly with ciliary body pigment epithelium. From the optic disc to the ora serrata, the sensory retina is continuous with the non-pigmented ciliary epithelium. Subretinal space is the potential space that exists between the neural retina and RPE [2]. Weak adhesion exists between the neural retina and RPE. At its anterior termination, the ora serrata, and at the margins of the optic nerve head, the neural retina is firmly affixed. The ora serrata is positioned 4-6 mm posterior to the ciliary epithelium and corresponds to the insertion of the medial and lateral rectus muscles. Ora serrata has a smooth temporal appearance but a serrated nasal appearance. Moreover, the retina is surrounded on its exterior by Bruch's membrane and on its interior by vitreous [3]. It is continuous posteriorly with the optic nerve, the site where ganglion cell axons leave the eye. Along the horizontal meridian, the human retina measures 32 millimeters from ora to ora, and its total surface area in each eye is approximately 1,100 square millimeters. The average thickness of the retina is 200 micrometers; it is slightly denser near the optic nerve head and the macula, and it thins out progressively at the ora serrata and fovea. Furthermore, the retinal surface can be divided into four zones known as Area centralis, Macula lutea, Fovea Centralis, and optical disc respectively. Additionally, photoreceptors, bipolar cells, and ganglion cells make up the majority of the neurosensory retina. Other essential neurons, such as amacrine cells and horizontal cells, have supporting functions. In three steps, photoreceptor cells, bipolar cells, and ganglion cells transport neural signals through the retina. Photoreceptors represent sensory receptors, whereas bipolar cells represent first-order cells and ganglion cells represent second-order neurons. . Additionally, the retina has ten layers [4], including nine layers of sensory retina and retinal pigment epithelium. RPE is developed embryologically from the outer layer of the optic cup, whereas photoreceptors are developed from the interior layer of the optic cup, and there is a potential space between the RPE and the sensory retina, known as the subretinal space . This imprecise attachment of RPE cells to photoreceptors is a result of the absence of specialized molecules such as laminin and fibronectin, [5] as well as junctional complexes between RPE cells and photoreceptors. The sensory retina detaches from the retinal pigment epithelium (RPE) in retinal detachment. During retinal detachment, RPE remains securely adhered to the choroid. On top of that, the Retina has dual circulation. The outer retinal layers obtain their blood supply from the choroidal circulation, while the inner retinal layers rely on the post retinal blood vessels of the central retinal vessels. The retinal circulation nourishes the retina up to the inner nuclear layer exclusively. It is believed that the outer plexiform layer receives nutrients from both retinal and choroidal vessels. The optic disc is where the central retinal artery, a branch of the ophthalmic artery, penetrates the retina. It divides into the upper and lower nasal and upper and lower temporal branches. The vessels of the retina are located in the nerve fiber layer just beneath the internal limiting membrane. However, the retina comprises of two types of capillary networks: the superficial network located in the nerve fiber layer or ganglion cell layer [6], whereas the deeper network located in the inner nuclear layer close to the outer plexiform layer. Within the optic nerve, the

central retinal artery has a well-developed tunica media composed of six layers of smooth muscle cells. As the artery leaves the optic nerve, its muscular sheathing is replaced by an incomplete layer of pericytes. Pericytes [7] are specialized mural cells that facilitate blood flow by contracting. Thus, the central retinal vessel remains artery and vein histologically for only a short distance from the optic disc, after which it transforms into arterioles and venules. However, the terms artery and vein are used in both clinical and histological contexts. Furthermore, retinal blood vessels lack an internal elastic lamina and are therefore unaffected by temporal arteritis. As part of the central nervous system, retinal vessels are typically end vessels that do not anastomose. However, anastomosis between the retinal vessels and the ciliary system of vessels occurs with the vessels that enter the optic nerve head near the lamina cribrosa from the circle of Zinn or Haler [8] . This arterial circle is formed by the anastomosis of two or four or more short posterior ciliary arteries and is located in the sclera surrounding the optic nerve. The only vessels in the body not controlled by the autonomic nervous system are the retinal vessels. The smooth muscles of blood vessels and the number of vasoactive mediators secreted by the vascular endothelium mediate autoregulation of retinal blood flow. Vasoconstriction [9] is caused by an increase in oxygen tension, while vasodilation is caused by an increase in intraocular pressure. Also comparable to the vasculature of the central nervous system the blood vessels of the retina are bordered by endothelium with extremely tight cellular junctions. The ratio of pericytes to endothelial cells in retinal capillaries is 1:1, thereby illustrating the sensitivity of the retinal blood vessels. The majority of problems induced by disorders affecting retinal blood vessels are due to clogging or leaking vessels. Therefore, if a retinal vein or artery becomes blocked, that portion of the visual field will be impaired indefinitely. This occurrence is commonly referred to as occlusion. There are many conventional deep learning various algorithms to examine and procure critical information regarding blood vessels in the retina, but none is more popular than a fully connected convolutional autoencoder, often known as UNet [10]. The suggested architecture is based on a fully convolutional network which has been modified and improved to operate with fewer training images and provide more accurate segmentations, thus enhancing our comprehension of the region of interest. In addition, the proposed architecture for Biomedical Image Segmentation was devised in 2015 at the University of Freiburg, Germany, by Olaf Ronneberger et al [11]. In addition, the suggested network's design can be summarized as a U-shaped encoder-decoder network architecture composed of four encoder blocks and four decoder blocks connected through a bridge which is typically a convolutional layer. By Doubling the number of feature channels, the encoder network diminishes the spatial dimensions by nearly half. However, the decoder network consists of half the number of feature channels, thereby restoring the original spatial dimension. In addition, the architecture's precise localization makes it superior to any typical convolutional neural network. During analysis, the suggested network provides crucial characteristics such as compatibility, customizability, and adaptability, among others.

II. Related work

U-Net topologies are prominent among Machine Learning researchers for segmenting biomedical images since they deliver precise results on challenging biomedical image datasets with relative ease. Furthermore, it has been established that these approaches provide comparable outcomes while consuming fewer resources. The research, which proposes an autonomous framework for segmentation of retinal blood vessels using a novel model dubbed weighted Res-UNet on two distinct datasets labeled DRIVE and STARE [12], yields comparable accuracies and sensitivities of 96.55%, 77.15%, and 96.93%, 74.66% respectively. In addition, the work which presents two novel effective strategies titled U-Net autoencoder and Fuzzy Classifier for segmentation of Retinal Blood vessels on the DRIVE database [13] achieves 95.72% accuracy with the Fuzzy system algorithm and 96.75% accuracy with the proposed U-Net autoencoder correspondingly. The study, which asserts a novel modified U-net architecture for segmentation of Retinal Blood vessels on four distinct databases labeled DRIVE, CHASE _DB1, STARE, and HRF [14], renders a diverse range of consistent sensitivity and specificity values respectively. In addition, the research reveals that the proposed method performs effectively on the dataset titled HRF in comparison to other versatile databases employed for this study. Moreover, the research which proposes a novel ensemble system framework housing a collection of bagged and boosted decision trees on a set of feature vectors based on the extracting the orientation, analysis of gradient vector field, morphological transformation, line strength measures, and Gabor filter responses from the datasets titled yields consistent accuracies of 94.56% and 94.93% on the presented databases titled DRIVE & STARE [15] respectively. Finally, the study which proposes an automatic retinal vessel segmentation framework with three distinct stages titled data preprocessing, data augmentation, and a fully convolutional neural network achieves average accuracies of 97.06%, 97.77%, and 97.73% when evaluated on the diverse datasets DRIVE, STARE, and CHASE_DB1 [16]. In addition, the research reveals that the proposed framework automatically and effectively performs retinal vessel segmentation on the presented datasets with ease.

III. Dataset

In this research, a bespoke database for segmenting retinal blood vessels was developed by integrating multiple prominent open-source datasets to promote heterogeneity and flexibility. In addition, the datasets 'ARIA', 'ChaseDB', 'DR-Hagis', 'DRIVE', 'HRF', 'IOSTAR', and 'ORVS' [17] were employed for model training and testing, whilst the dataset 'STARE' [18] were utilized for model validation. In addition, each discrete dataset employed form model training comprises of approximately 20 to 30 exceptional fluorescein angiography (fundus) scans with their respective masks spread across the folders titled train and test respectively, resulting in a custom training database housing approximately of 760 fluorescein angiography (fundus) scans and their corresponding masks for model analysis. Finally, the dataset dubbed 'STARE' comprises of roughly 397 exemplary fluorescein angiography (fundus) scans from which five fundus scans selected at random make up the validation database for model validation.

IV. Model Description

In order to effectively segment the retinal blood vessels on any given fundus scan with ease ,the proposed project presents

a distinct UNet model framework comprising of four distinct phases [19] titled 'Data Acquisition', 'Data Modelling & Augmentation', 'Model Initialization and Hyperparameter Optimization', and 'Final Model Training and Evaluation'.

A. Data Acquisition

This phase outlines the arduous process of acquiring and characterizing the nature of the diverse datasets employed for training and assessing the efficacy of the proposed model framework.

B. Data Modelling & Augmentation

This phase focuses on automating the preprocessing and augmentation of images available in the raw database obtained in the previous phase. In addition, the proposed phase consists of four distinct phases [20] titled Image resizing, Image Colorization and Formatting, Image Augmentation, and Model Construction & Loss Computation Scripts. respectively.

a) Image Resizing:

Prior to model training and validation, the proposed stage attempts to resize the images and their corresponding masks to an average size of 512 by 512 pixels [21] to ensure data uniformity.

b) Image Colorization & Formatting:

This stage seeks to colorize processed images and their respective masks in RGB and greyscale color formats [22], respectively. In addition, the processed images were saved separately with the universal file extension 'Portable Network Graphics'.

c) Image Augmentation:

The proposed stage seeks to supplement the preprocessed images and their corresponding masks with a distinct set of data augmentation [23] techniques known as Horizontal Flip, Vertical Flip, Elastic Transform, Grid Distortion, and Optical Distortion respectively. In addition, this approach was taken to exploit the symmetric nature of the images and their corresponding masks, thereby enhancing the model's capacity for perception and extension. Finally, this phase was exclusively applied to datasets labeled for model training and validation, and not real time validation (RTV).

d) Model Construction & Loss Computation Scripts:

This stage aims to establish two discrete Python scripts titled model.py and metrics.py that have been developed using TensorFlow [24]. Furthermore, the script titled model.py houses a comparable UNet model comprising of four distinct encoder and decoder blocks [25] connected by a single convolution block that serves as the model's bottleneck layer. In addition, the proposed convolution block encompasses two convolutional layers, each with a Scaled Exponential Linear Unit or 'SELU' activation function and a LeCun initializer [26] . Moreover, each combination of encoder and decoder blocks incorporates a distinctive set of convolution blocks with a discrete set of input features. As the model's output layer, a single convolutional Layer with a single neuron and sigmoid activation function [27] serves as the final layer. Finally, the script dubbed metrics.py features five configurable segmentation metrics [28] titled Precision, Recall, Dice Coefficient, Dice Loss, and Intersection Over Union , which are solely computed for augmenting the proposed model's performance as a whole.

C. Model Initialization & Hyperparameter Optimization

This phase outlines the cumbersome process of troubleshooting issues encountered during training and testing the distinct UNet model framework on the presented training database. In addition, this phase includes the challenge of identifying suitable hyperparameters [29] to enhance the generalization capability of a comparable model for validation analysis.

D. Final Model Training and Evaluation

This phase describes the process of training and validating an analogous UNet model framework retrofitted with distinct hyperparameters [30] (obtained in the previous phase) on the processed training and validation databases, respectively. Figure 1 illustrates the proposed project framework while Figures 2 & 3 depict the proposed UNet model architecture and proposed project workflow respectively.

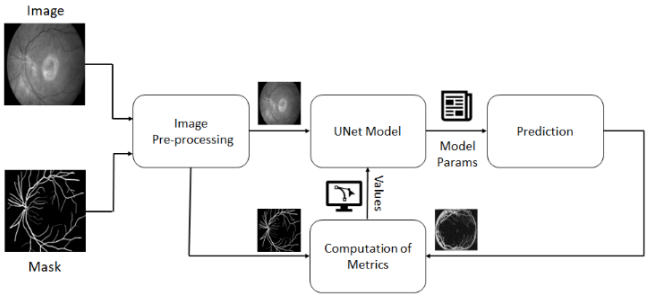

Fig. 1: Proposed Project Framework

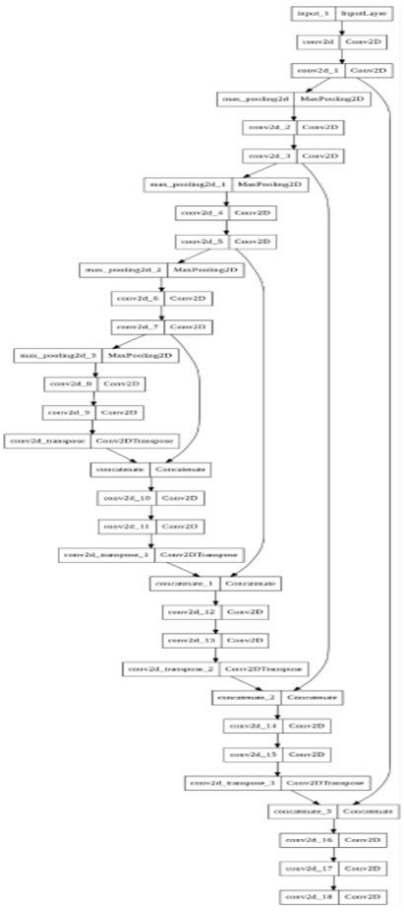

Fig. 2: Proposed UNet Model Architecture

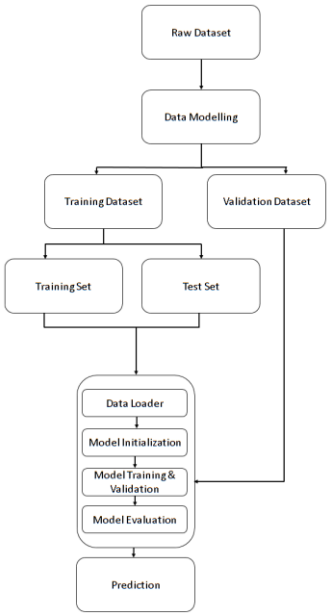

Fig. 3: Proposed Project Workflow

V. Experiments & Evaluation

In this research, a proposed hypertuned UNet model framework comprising of a comparable UNet model, composed of four encoder and decoder blocks connected via a fully connected convolution layer, which serves as the model's bottleneck layer was presented. Moreover, the suggested convolution block consists of two convolutional layers, each with a Scaled Exponential Linear Unit or 'SELU' activation function and a LeCun initializer. In addition, each combination of encoder and decoder blocks comprises a unique set of convolution blocks with a distinct set of input features. A single convolutional Layer with a single neuron and sigmoid activation function serves as the model's output layer. In addition, the aforementioned model framework was evaluated using the criterion 'Binary Categorical Cross Entropy' [31] and an optimizer 'Adaptive Moment Estimation' or ADAM [32] with a fixed learning rate of 1e-4 . Moreover, the suggested model framework was evaluated using a fixed batch size of 16 and a fixed number of 100 epochs. Finally, the proposed model framework was tuned with a criterion titled Early Stopping [33] , which aims in drastically reducing temporal and spatial complexity for a given model by limiting the effective number of epochs to a bare minimum.so in the case of this project the presented model framework was evaluated using 40 epochs. Furthermore, the aforementioned model framework was finalized upon conducting a series of novel experiments using the same hyper parameters with minor modifications on the presented custom database. Initially, a distinct model framework comprising of a rudimentary UNet model framework with two encoder and decoder blocks [34] was initially tested. Experiment results indicated that the proposed model framework was susceptible to a condition referred to as overfitting, primarily due to the fact that the aforementioned model was too simplistic. Moreover, a second experiment involving a unique framework featuring a similar UNet model framework comprising of four encoder and decoder blocks adjusted with the activation function was also conducted. Experiment results indicated that the aforementioned framework featuring the model was performing adequately; however, the model exhibited higher time complexity due to the model's lengthy convergence time to an optimal solution. Furthermore, an experiment involving a novel framework featuring a similar UNet model framework comprising of four encoder and decoder blocks adjusted with a Scaled Exponential Linear Unit OR 'SELU' activation function was tested. In addition, the model's final layer incorporates two neurons with a SoftMax activation function [35]. In addition, the proposed model's criterion was modified from Binary Cross Entropy to Categorical Cross Entropy [36]. The experimental results indicated that the aforementioned model framework exhibited greater time complexity and greater loss than normal. Finally, a distinct experiment incorporating a novel framework comprising a UNet model framework consisting of four encoder and decoder blocks adjusted with a Scaled Exponential Linear Unit OR 'SELU' activation function was trained and validated on the presented database using a versatile loss metric titled 'BCE_Dice_loss' [37]. In addition, the distinct loss metric was computed by summing the losses titled dice loss and binary cross entropy loss. Experiment results indicated that the proposed framework for the model exhibited poorer visualization results than normal. In addition, the aforementioned list of experiments, followed by the final model training and validation, were conducted in a multi-GPU environment [38] with 100 GB of RAM, 2 CPU cores, and 5 GPU cores respectively.

VI. Model Evaluation

The proposed hypertuned UNet model framework was primarily evaluated using distinct segmentation metrics.The metrics utilized for evaluating the proposed phases are given by Dice Coefficient, Dice Loss, Precision, Recall & Intersection Over Union respectively [39]. The metrics were computed using equations (1) to (4).

$$Precision = \frac{TP}{TP+FP} \quad \text{-(1)}$$

$$Recall = \frac{TP}{TP+FN} \quad \text{-(2)}$$

$$Dice\ Loss = 1 - \frac{2*|X \cap Y|}{|X|+|Y|} \quad \text{-(3)}$$

$$Dice\ Coefficient = \frac{2*|X \cap Y|}{|X|+|Y|} \quad \text{-(4)}$$

$$Intersection\ Over\ Union = \frac{Area\ of\ Overlap}{Area\ of\ Union} \quad \text{-(5)}$$

The precision score or PPV for the model was computed by substituting the values of True Positive (TP) and False Positive (FP) in equation (1). Moreover, the recall score or TPR for the model was compiled by substituting the values of True Positive (TP) and False Negative (FN) in equation (2).The Dice Coefficient for the model was quantified by substituting the values of Area of Overlap (i.e. Intersection between the images) and total number of pixels present between the two images in equation(4). In addition, the dice loss was computed by subtracting one from the obtained dice coefficient as illustrated in equation(3) .Finally, the intersection over union (iou) for the model was obtained by plugging the values of the following components: overlap of the ground truth and projected region verified by the model into equation (5).

VII. Model Results

This phase evaluates the effectiveness of the proposed hypertuned UNet model framework trained and validated on a multi-GPU framework, with hyper parameters optimized by a proprietary technique [40]. Additionally, the efficacy of the proposed model was assessed using the predetermined segmentation metrics. Figures 4, 5, 6 and 7 illustrate the respective metric results obtained during model training and validation.

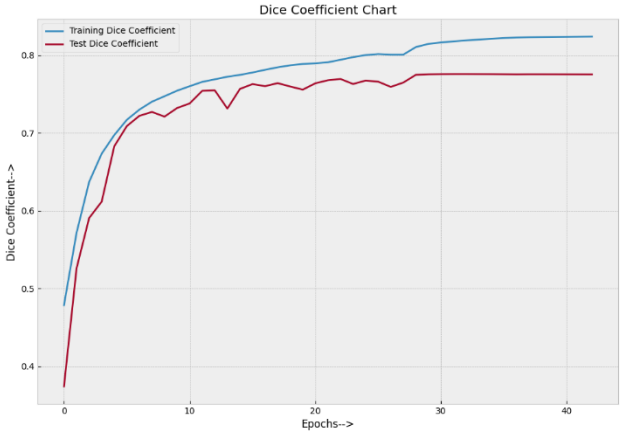

Fig. 4: Dice Coefficient recorded upon training and validating the proposed hypertuned UNet model framework.

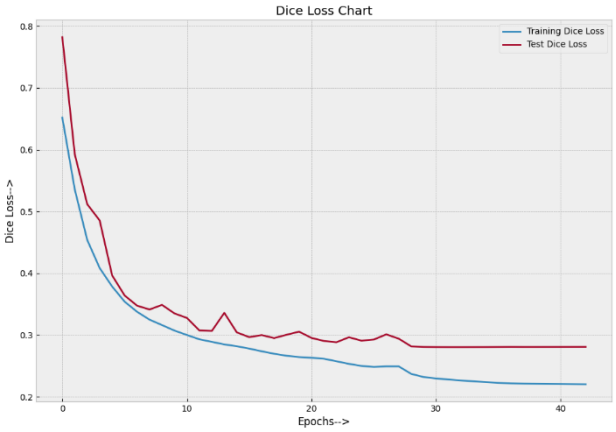

Fig. 5: Dice Loss recorded upon training and validating the proposed hypertuned UNet model framework.

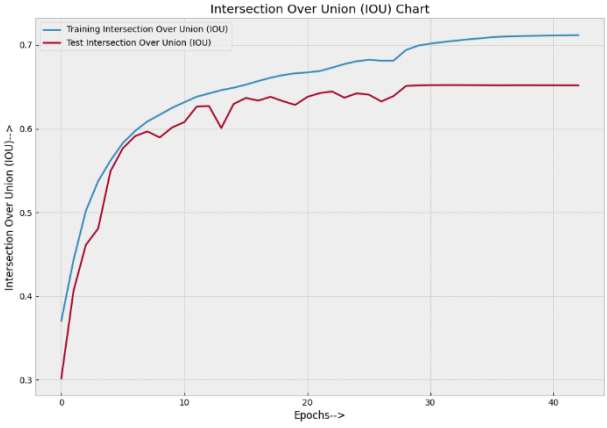

Fig. 6: Intersection Over Union (IOU) Score recorded upon training and validating the proposed hypertuned UNet model framework.

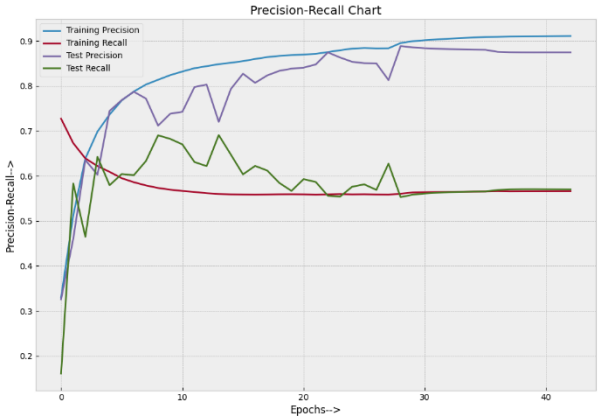

Fig. 7: Precision & Recall Scores recorded upon training and validating the proposed hypertuned UNet model framework.

Finally, Figure 8 depicts the visual results recorded upon evaluating the proposed hypertuned UNet model framework on a comparable validation dataset.

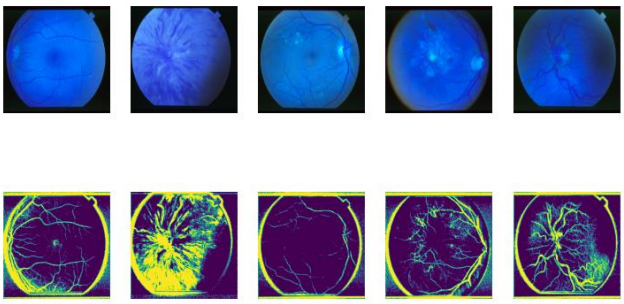

Fig. 8: Visual Results recorded upon validating the proposed hypertuned UNet model framework.

VIII. Conclusion

This study highlights the significance of discerning and segmenting retinal blood vessels dispersed all over the retina by employing a unique model framework titled hypertuned UNet. Furthermore, the work demonstrates and investigates the benefits of the proposed strategy on an extensive variety of exceptional fundus scan databases. In addition, the study also illustrates the benefits of training and validating the proposed hypertuned UNet model framework on a Multi GPU Framework. Based on the results presented, it is possible to infer that the proposed hypertuned UNet model framework trained and validated on a multi-GPU framework delivers optimum results with minimal temporal and spatial complexity respectively.

In the future, the proposed model framework will undergo testing on comparable but exclusive datasets, fostering model heterogeneity while upholding model integrity.

References

[1] Hou, Yuchen, Junde Li, Jungjin Yoon, Abbey Marie Knoepfel, Dong Yang, Luyao Zheng, Tao Ye, Swaroop Ghosh, Shashank Priya, and Kai Wang. "Retina-inspired narrowband perovskite sensor array for panchromatic imaging." Science Advances 9, no. 15 (2023): eade2338.

[2] Hunt, Nicola C., Dean Hallam, Valeria Chichagova, David H. Steel, and Majlinda Lako. "The application of biomaterials to tissue engineering neural retina and retinal pigment epithelium." Advanced healthcare materials 7, no. 23 (2018): 1800226.

[3] Mishra, Deepakkumar, Shilpkala Gade, Katie Glover, Ravi Sheshala, and Thakur Raghu Raj Singh. "Vitreous humor: composition, characteristics and implication on intravitreal drug delivery." Current eye research 48, no. 2 (2023): 208-218.

[4] Zhang, Yiheng, Zhongliang Li, Nan Nan, and Xiangzhao Wang. "TranSegNet: Hybrid CNN-Vision Transformers Encoder for Retina Segmentation of Optical Coherence Tomography." Life 13, no. 4 (2023): 976.

[5] Aleman, John D., Christian D. Young, Sana D. Karam, and Xiao‐Jing Wang. "Revisiting laminin and extracellular matrix remodeling in metastatic squamous cell carcinoma: What have we learned after more than four decades of research?." Molecular Carcinogenesis 62, no. 1 (2023): 5-23.

[6] Ghita, Aurelian Mihai, Daniela Adriana Iliescu, Ana Cristina Ghita, Larisa Adriana Ilie, and Alexandru Otobic. "Ganglion Cell Complex Analysis: Correlations with Retinal Nerve Fiber Layer on Optical Coherence Tomography." Diagnostics 13, no. 2 (2023): 266.

[7] Longden, Thomas A., Guiling Zhao, Ashwini Hariharan, and W. Jonathan Lederer. "Pericytes and the Control of Blood Flow in Brain and Heart." Annual Review of Physiology 85 (2023): 137-164.

[8] Fan Gaskin, Jennifer C., Manisha H. Shah, and Elsa C. Chan. "Oxidative stress and the role of NADPH oxidase in glaucoma." Antioxidants 10, no. 2 (2021): 238.

[9] Ribas, Michelle Zonkowski, Gabriela Ferreira Paticcié, Sara Diógenes Peixoto de Medeiros, Arthur de Oliveira Veras, Felipe Micelli Noleto, and Júlio César Claudino Dos Santos. "Reversible cerebral vasoconstriction syndrome: literature review." The Egyptian Journal of Neurology, Psychiatry and Neurosurgery 59, no. 1 (2023): 5.

[10] https://doi.org/10.48550/arXiv.1505.04597

[11] Lopes, Daniel, Luís Coelho, and Manuel F. Silva. "Development of a Collaborative Robotic Platform for Autonomous Auscultation." Applied Sciences 13, no. 3 (2023): 1604.

[12] X. Xiao, S. Lian, Z. Luo and S. Li, "Weighted Res-UNet for High-Quality Retina Vessel Segmentation," 2018 9th International Conference on Information Technology in Medicine and Education (ITME), Hangzhou, China, 2018, pp. 327-331, doi: 10.1109/ITME.2018.00080.

[13] T. Mostafiz, I. Jarin, S. A. Fattah and C. Shahnaz, "Retinal Blood Vessel Segmentation Using Residual Block Incorporated U-Net Architecture and Fuzzy Inference System," 2018 IEEE International WIE Conference on Electrical and Computer Engineering (WIECONECE), Chonburi, Thailand, 2018, pp. 106-109, doi: 10.1109/WIECONECE.2018.8783182.

[14] Afolabi, Oluwatobi & Nelwamondo, Fulufhelo & Mabuza, Gugulethu. (2020). Blood Vessel Segmentation from Fundus Images Using Modified U-net Convolutional Neural Network. Journal of Image and Graphics. 8. 21-25. 10.18178/joig.8.1.21-25.

[15] M. M. Fraz et al., "An Ensemble Classification-Based Approach Applied to Retinal Blood Vessel Segmentation," in IEEE Transactions on Biomedical Engineering, vol. 59, no. 9, pp. 2538-2548, Sept. 2012, doi: 10.1109/TBME.2012.2205687.

[16] Jiang, Yun, Hai Zhang, Ning Tan, and Li Chen. 2019. "Automatic Retinal Blood Vessel Segmentation Based on Fully Convolutional Neural Networks" Symmetry 11, no. 9: 1112. https://doi.org/10.3390/sym11091112

[17] Galdran, Adrian, André Anjos, José Dolz, Hadi Chakor, Hervé Lombaert, and Ismail Ben Ayed. "The little w-net that could: state-of-the-art retinal vessel segmentation with minimalistic models." arXiv preprint arXiv:2009.01907 (2020).

[18] Krestanova, Alice, Jan Kubicek, and Marek Penhaker. "Recent techniques and trends for retinal blood vessel extraction and tortuosity evaluation: a comprehensive review." Ieee Access 8 (2020): 197787-197816.

[19] Albatayneh, Omar, Lars Forslöf, and Khaled Ksaibati. "Image retraining using TensorFlow implementation of the pretrained inception-v3 model for evaluating gravel road dust." Journal of Infrastructure Systems 26, no. 2 (2020): 04020014.

[20] Khanna, Anita, Narendra D. Londhe, S. Gupta, and Ashish Semwal. "A deep Residual U-Net convolutional neural network for automated lung segmentation in computed tomography images." Biocybernetics and Biomedical Engineering 40, no. 3 (2020): 1314-1327.

[21] Abed, Mohammed K., Marwah M. Kareem, Raed Khalid Ibrahim, Mohammed M. Hashim, Sefer Kurnaz, and Adnan Hussein Ali. "Secure medical image steganography method based on pixels variance value and eight neighbors." In 2021 International Conference on Advanced Computer Applications (ACA), pp. 199-205. IEEE, 2021.

[22] Qi, Lei, Lei Wang, Jing Huo, Yinghuan Shi, and Yang Gao. "GreyReID: A novel two-stream deep framework with RGB-grey information for person re-identification." ACM Transactions on Multimedia Computing, Communications, and Applications (TOMM) 17, no. 1 (2021): 1-22.

[23] Liu, Xinyu, Haiting Shen, Long Gao, and Rui Guo. "Lung parenchyma segmentation based on semantic data augmentation and boundary attention consistency." Biomedical Signal Processing and Control 80 (2023): 104205.

[24] Momin, Ahad. "Image Segmentation Using Deep Learning Tensorflow and Keras Implementation in Python." (2020).

[25] Tiwari, Twinkle, and Mukesh Saraswat. "A new modified-unet deep learning model for semantic segmentation." Multimedia Tools and Applications 82, no. 3 (2023): 3605-3625.

[26] Madasu, Avinash, and Vijjini Anvesh Rao. "Effectiveness of self normalizing neural networks for text classification." In Computational Linguistics and Intelligent Text Processing: 20th International Conference, CICLing 2019, La Rochelle, France, April 7–13, 2019, Revised Selected Papers, Part II, pp. 412-423. Cham: Springer Nature Switzerland, 2023.

[27] Salaheddine, Friki Imed. "Convolutional Neural Networks (CNN): Models and Algorithms." In Advanced Bioinspiration Methods for Healthcare Standards, Policies, and Reform, pp. 97-120. IGI Global, 2023.

[28] Isensee, Fabian, Paul F. Jäger, Peter M. Full, Philipp Vollmuth, and Klaus H. Maier-Hein. "nnU-Net for brain tumor segmentation." In Brainlesion: Glioma, Multiple Sclerosis, Stroke and Traumatic Brain Injuries: 6th International Workshop, BrainLes 2020, Held in Conjunction with MICCAI 2020, Lima, Peru, October 4, 2020, Revised Selected Papers, Part II 6, pp. 118-132. Springer International Publishing, 2021.

[29] Morteza, Azita, Amir Abbas Yahyaeian, Marzieh Mirzaeibonehkhater, Sina Sadeghi, Ali Mohaimeni, and Saman Taheri. "Deep Learning Hyperparameter Optimization: Application to Electricity and Heat Demand Prediction for Buildings." Energy and Buildings (2023): 113036.

[30] Patil, Sakshee, Ankur Miglani, Pavan Kumar Kankar, and Debanik Roy. "Deep learning-based methods for detecting surface defects in steel plates." In Smart Electrical and Mechanical Systems, pp. 87-107. Academic Press, 2022.

[31] Brahmbhatt, Prashant, and Siddhi Nath Rajan. "Skin lesion segmentation using SegNet with binary CrossEntropy." In Proceedings of the International Conference on Artificial Intelligence and Speech Technology (AIST2019), Delhi, India, pp. 14-15. 2019.

[32] ŞEN, Sena Yağmur, and Nalan ÖZKURT. "Convolutional neural network hyperparameter tuning with adam optimizer for ECG classification." In 2020 Innovations in Intelligent Systems and Applications Conference (ASYU), pp. 1-6. IEEE, 2020.

[33] Ferro, Manuel Vilares, Yerai Doval Mosquera, Francisco J. Ribadas Pena, and Víctor M. Darriba Bilbao. "Early stopping by correlating online indicators in neural networks." Neural Networks 159 (2023): 109-124.

[34] Ullah, Ihsan, Farman Ali, Babar Shah, Shaker El-Sappagh, Tamer Abuhmed, and Sang Hyun Park. "A deep learning based dual encoder–decoder framework for anatomical structure segmentation in chest X-ray images." Scientific Reports 13, no. 1 (2023): 791.

[35] Hossain, Shahriar, Amitabha Chakrabarty, Thippa Reddy Gadekallu, Mamoun Alazab, and Md Jalil Piran. "Vision transformers, ensemble model, and transfer learning leveraging explainable ai for brain tumor detection and classification." IEEE Journal of Biomedical and Health Informatics (2023).

[36] Amin, Belal, Romario Sameh Samir, Youssef Tarek, Mohammed Ahmed, Rana Ibrahim, Manar Ahmed, and Mohamed Hassan. "Brain tumor multi classification and segmentation in MRO images using deep learning." arXiv preprint arXiv:2304.10039 (2023).

[37] Xu, Hongzhang, Hongjie He, Ying Zhang, Lingfei Ma, and Jonathan Li. "A comparative study of loss functions for road segmentation in

remotely sensed road datasets." International Journal of Applied Earth Observation and Geoinformation 116 (2023): 103159.

[38] Berral, Josep Ll, Oriol Aranda, Juan Luis Dominguez, and Jordi Torres. "Distributing Deep Learning Hyperparameter Tuning for 3D Medical Image Segmentation." In 2022 IEEE International Parallel and Distributed Processing Symposium Workshops (IPDPSW), pp. 1045-1052. IEEE, 2022.

[39] Awan, Mazhar Javed, Mohd Shafry Mohd Rahim, Naomie Salim, Amjad Rehman, and Begonya Garcia-Zapirain. "Automated knee MR images segmentation of anterior cruciate ligament tears." Sensors 22, no. 4 (2022): 1552.

[40] Onzon, Emmanuel, Fahim Mannan, and Felix Heide. "Neural auto-exposure for high-dynamic range object detection." In Proceedings of the IEEE/CVF conference on computer vision and pattern recognition, pp. 7710-7720. 2021.